Stabilizing Thin Film Polymer Bilayers against Dewetting Using Multiwalled Carbon Nanotubes

Jaseung Koo,[†] Kwanwoo Shin,*[,||] Young-Soo Seo,[⊥] Tadanori Koga,[‡] Seongchan Park,[†] Sushil Satija,[#] Xuming Chen,[§] Kyunghwan Yoon,[§] Benjamin S. Hsiao,[§] Jonathan C. Sokolov,[†] and Miriam H. Rafailovich*[,‡]

Department of Materials Science and Engineering, Chemical and Molecular Engineering Program, and Department of Chemistry, State University of New York at Stony Brook, Stony Brook, New York 11794, Department of Chemistry, Sogang University, Seoul 121-742, South Korea, Department of Nano Science & Technology, Sejong University, Seoul 143747, South Korea, and Center for Neutron Research, National Institute of Standards and Technology, Gaithersburg, Maryland 20899

Received July 12, 2007; Revised Manuscript Received October 9, 2007

ABSTRACT: We have investigated the effect of the length of multiwalled carbon nanotubes (MWNT) on the dewetting dynamics of thin polymer films. The results indicated that long nanotubes were much more effective than short nanotubes in stabilizing the films against dewetting. The diffusion of polymer chains in the filled matrices was measured using neutron reflectivity, and the result indicated no significant effect on the diffusion coefficient by either short or long nanotubes. We therefore proposed a model whereby the nanotubes did not interact with the individual polymer chains. On the other hand, the long nanotubes formed an effective entangled network, which prevented long-range motion of the polymer films upon dewetting. This model was supported by rheological experiments on bulk samples where the nanotubes had a strong effect on G' of the polymer and only a negligible effect on G''.

Introduction

Thin polymer multilayer films are increasingly being used for numerous applications ranging from dielectric and optical coatings to electronic packaging.[1−3] Because most polymers are immiscible, the interfacial tension between the layers can be unfavorable leading to dewetting.[4] Recently, several research groups have demonstrated that the addition of nanoparticles into the matrix can control dewetting.[5−8] Barnes et al.[5] have shown that the addition of fullerene (C_{60}) fillers can stabilize homopolymer films against dewetting due to surface interactions between the silicon substrates and the particles that can pin the polymer chains. Xavier et al.[6] demonstrated that dewetting can also be controlled even in the case when particles/matrix interactions were unfavorable simply by controlling the relative size of the particles and the polymer chains. Here, we demonstrate that the aspect ratio of the filler can also affect dewetting by changing the rheology of the dewetting layer.

Fullerene pipes or carbon nanotubes (CNTs), consisting of the same chemical structure as the C_{60}, have received considerable attention due to their unique rheological properties.[9−11] Du et al.[10] investigated the influence of the single-walled nanotubes (SWNT) on the viscoelastic properties of the composites. They reported that at low frequencies, they found an increase in the storage modulus (G') for concentrations as low as 0.5% (by weight), while at high frequencies, G' was unaffected even by the addition of 2% (by weight) SWNTs. They attributed this behavior to network formation, which yielded a gel-like rheological response and hence was able to explain the enhancement in the flame retardant behavior they observed.[11] Here, we propose that the network formation may also enhance the stability of thin films containing nanotubes against dewetting.

In this work, therefore, we study the effect of nanotube length and nanotube loading on the dewetting behavior of polymer thin films and correlate the results with diffusion measurements where single chain dynamics are measured. To probe the hypothesis of network formation, we also investigate the differences between films containing long entangled MWNTs (*l*-MWNTs) and short straight MWNTs (*s*-MWNTs), which cannot form networks. We show that the *l*-MWNTs are more effective at stabilizing the films, while neither short nor long MWNTs affect the diffusion of individual polymer chains. To compare with bulk phenomena, rheological measurements were also performed on melt blended samples containing *s*-MWNTs and *l*-MWNTs. The results confirm the previously suggested model[10,12] for formation of a nanotube network where the mesh size can be an important factor in the polymer dynamics.

Experimental Section

Materials. Commercially available multiwall carbon nanotube (MWNT) (Nanostructured & Amorphous Materials, Inc., USA), and polystyrene (PS) and poly(methyl methacrylate) (PMMA), as well as their deuterated analogues, were used in these experiments. The specifications regarding the polymers used are listed in Table 1.

Purified MWNT. MWNTs were produced by the chemical vapor deposition (CVD) method. The nanotubes have an average diameter $d_c = 25 \pm 5$ nm. The MWNTs were purified by the oxidizing acid treatment method developed by Smalley et al.[13] MWNTs (100 mg) were immersed in 100 mL of concentrated 3:1 solutions of sulfuric acid (H_2SO_4) and nitric acid (HNO_3). The MWNT suspended solutions were kept in an ultrasonicator (Bran-

* Corresponding authors. E-mail: kwshin@sogang.ac.kr (K.S.); mrafailovich@notes.cc.sunysb.edu (M.H.R.).
[†] Department of Materials Science and Engineering, State University of New York at Stony Brook.
[‡] Chemical and Molecular Engineering Program, State University of New York at Stony Brook.
[§] Department of Chemistry, State University of New York at Stony Brook.
[||] Sogang University.
[⊥] Sejong University.
[#] NIST.

10.1021/ma071550l CCC: $37.00
Published on Web 11/30/2007

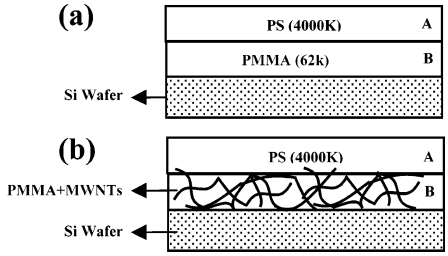

Figure 1. Schematic of the sample geometry for the dewetting experiments. (a) A liquid PMMA layer, B, is spun-cast onto the substrate. A more viscous PS layer, A, is floated on top of the bottom layer. (b) To investigate the effect of MWNTs on dewetting dynamics, the bottom PMMA layer is filled with nanotubes.

Table 1. Characteristics of Polymers Used in This Study

	sample	M_w	M_w/M_n	source
dewetting	PS	4 000 000	1.05	polymer source
	PMMA	62 000	1.07	polymer source
diffusion	PMMA	85 000	1.09	polymer source
	*d*PMMA	86 500	1.13	polymer source
bulk rheology	PMMA	100 000	~3	Polysciences

sonic Co.) for 3 h at 70 °C, followed by stirring first for 5 h at 55 °C, and then for 43 h at 35 °C. To produce the shorter multiwalled nanotubes (*s*-MWNTs), further sonication was applied for another 2 days at 70 °C in acid solution. The acid-treated MWNTs suspension was diluted with 150 mL of deionized (DI) water and filtered in a 0.1 μm PVDF membrane (Millipore, USA). In the final step of purification, we added hydrochloric acid (HCl) to terminate with carboxylic acid groups rather than carboxylate groups at the opened ends of the purified MWNTs. The MWNT suspension was filtered several times to remove the acid, followed by drying under the vacuum at 80 °C overnight, grinding every hour to obtain a fine powder.

Sample Preparation. PMMA was chosen as the bottom layer because the more polar PMMA is known to segregate preferentially to the Si interface.[16] The sample geometry is shown in Figure 1. PMMA (M_w = 62K, M_w/M_n = 1.07) and oxidized MWNT were dispersed in the dimethylformamide (DMF) (Aldrich), in ratios ranging from 0.02% to 1% by weight of MWNT. The solutions were clear and stable for at least 1 month, indicating that the nanotubes were well dispersed in the PMMA solution, during the time of the experiment.

Polished 200 μm thick Si (100) wafers were purchased from Wafer World (West Palm Beach, FL) and partitioned to 2 × 2 cm^2 samples. The surfaces were treated with a modified Shiraki technique: the substrates were immersed in H_2O:H_2O_2:H_2SO_4 (3:1:1 vol) for 10 min at 80 °C, rinsed in deionized water, and immersed in H_2O:HF (5:1 vol) for 30 s at room temperature to remove organic residue.

The solution was heated to 80 °C before spinning to increase the evaporation rate of the DMF, which is necessary to produce high-quality films. The warm solution containing the nanotubes was rapidly spun-cast onto HF etched Si wafers. The samples were then annealed at 130 °C in a vacuum of 10^{-3} Torr for 3 h to remove the residual solvent and relax strains induced by the spinning process. The thickness of the layers, 1100 ± 50 Å, was measured using ellipsometry. PS (M_w = 4000K, M_w/M_n = 1.05) dissolved in toluene was spun-cast onto a glass slide (a film is 350 ± 20 Å thick) and carefully floated from DI water onto the PMMA substrate (these molecular weights were chosen such that the conditions for plug flow dewetting specified in ref 4 were met). Control samples, on substrates without nanotubes, were prepared using the same procedure. After preparation, the films were allowed to dry at room temperature overnight before annealing. To initiate dewetting, the PS/PMMA bilayer samples were annealed at a fixed temperature of 195 °C in a high-vacuum oven where the vacuum was maintained at 10^{-7} Torr at all times. The samples were then quenched to room temperature, and the diameters of the dewetting holes were measured by using an Olympus optical microscope. To measure the detailed morphology of the dewetting holes, we also used an atomic force microscope (AFM) (Digital Instruments, USA) with a silicon nitride tip. The underlying structure of the substrates after the dewetting occurred was measured by placing them in cyclohexane for 10 min, which dissolved only the PS layer.

Neutron Reflectivity. The specular neutron reflectivity (NR) experiments were conducted with the NG7 reflectometer at the Cold Neutron Facility of the National Institute of Standards and Technology (Gaithersburg, MD) with a wavelength (λ) of 4.76 Å and $\Delta\lambda/\lambda \approx 0.025$. The vertical slits were adjusted as a function of the scattering wave-vector transfer (q_z) to fix the resolution at a constant value of $\Delta q_z/q_z \approx 0.03$, while the size of the horizontal slits was set to 30 mm. The NR was measured as a function of $q_z = (4\pi/\lambda \sin\theta)$, where θ is the grazing angle of incidence. The samples were placed in a high-vacuum, temperature-controlled chamber, specially designed for NR experiments.

The modeling and fitting of the reflectivity were carried out based on an error-function model density profile $\rho(z)$ perpendicular to the sample surface. The physical quantities to fit the data are the thicknesses, the interfacial root-mean-square (rms), roughness (σ), and the scattering length density (SLD) corresponding to the elastic coherent-scattering per unit volume, which is crucial for the study of the multilayer system. To provide a good contrast between the polymer−polymer interface, deuterated poly(methyl methacrylate) (*d*PMMA) was used in neutron reflectivity studies.

For the sample preparation, a blend of 60% PMMA (M_w = 85K) + 40% *d*PMMA (M_w = 86.5K) was first dissolved in toluene, and then a suspension of MWNTs (0.5 mg/mL) in DMF was added in the polymer matrix (in the ratio of 0.2% by weight of MWNTs) where the final volume fraction of DMF is assured to be less than 10%. This solution was then spun-cast onto the surface of a thick Si wafer, and the second layer of the PMMA (M_w = 85K, M_w/M_n = 1.09) with the same amount of nanotubes was also spun-cast onto a clean glass slide and carefully floated from DI water onto the bottom layer substrate.

Bulk Rheological Measurement. The PMMA for the polymer matrix was purchased from Polysciences (M_w = 100K, PDI = 3.0). The nanocomposites were prepared by the coagulation method.[17] *s*-MWNTs (the mean length = 310 nm) and *l*-MWNTs (the length >2 μm) were dispersed in DMF (1 mg/mL) with an ultrasonication for 30 min. Based on the desired weight percentage, an appropriate quantity of PMMA was dissolved in the nanotube suspension, and DMF was added to the MWNT/PMMA mixture to give a final concentration of 50 mg/mL. Subsequently, the suspension was dropped into the deionized water with stirring (a volume ratio of the suspension and water is 1 to 10). The precipitated PMMA/MWNT mixture was collected on the cellulose filter paper (Whatman, USA) and dried overnight in a vacuum at 120 °C. The dry powder was mixed again using a Brabender twin-screw melt-mixer at 180 °C with a mixing speed of 100 rpm for 10 min to improve dispersion. For the rheological samples, we placed the mixture samples in 25 mm diameter, 1.5 mm thick, cylindrical molds of stainless steel covered with heat resistant Kapton films and pressed for 20 min at 180 °C. Small strain oscillatory rheological measurements were carried out using a Physica MCR 301 strain-controlled rheometer, manufactured by Anton-Paar (USA). A constant strain amplitude (0.5%) was applied in all dynamic measurements. All measurements of the frequency sweep ($0.01 < \omega < 10$ rad/s) were performed at 200 °C under the flow of nitrogen to avoid the degradation of polymer matrices.

Tunneling Electron Microscopy (TEM) Characterization. TEM analysis was performed on a Philips CM12 TEM operation at 100 keV. The sample was prepared by spin casting the PMMA solution containing 1 wt % *l*-MWTNs on the Si wafers and was annealed at 175 °C for 5 h. The films were then floated from the sodium hydroxide solution onto carbon-coated Cu grids and dried under the vacuum at room temperature for 2 days. Figure 2a shows TEM images of the thin films where we can see that the length is indeed longer than 2 μm, forming an overlapping network, but a little amount of the catalysts (or impurities) still remained even

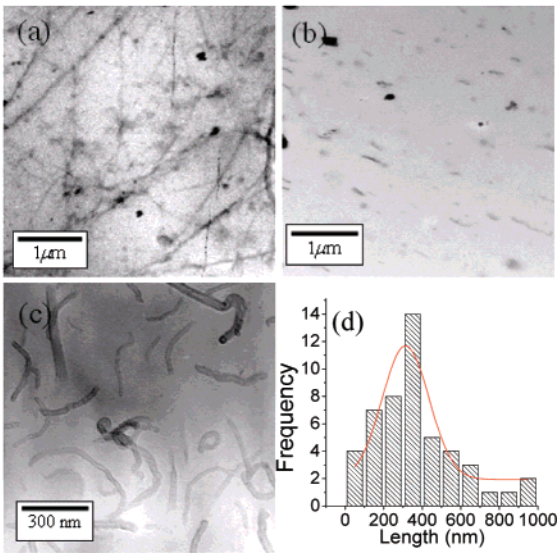

Figure 2. TEM images of (a) 1% *l*-MWNTs (by weight) in the PMMA film after annealing for 5 h at 175 °C, (b) 0.5% *s*-MWNTs (by weight) in the PMMA bulk, (c) *s*-MWNTs deposited on TEM grid, and (d) their length distribution histogram.

after the purification. We also prepared the TEM sample for the *s*-MWNTs by dropping the nanotube suspension (0.2 mg/mL) in DMF on the carbon-coated Cu grid, followed by drying it in the vacuum at room temperature for 2 days. Figure 2d is a histogram of the length measured from Figure 2c, where we found that the mean length is 313 ± 23 nm, which is significantly shorter than *l*-MWNTs. To check the dispersion of the s-MWNTs in the PMMA bulk, we melt-mixed the PMMA with 0.5 wt % of *s*-MWNTs and sliced the samples into thin films (around 100 nm thick) at room temperature, using a Reichert-Jung Ultracut E microtome with a diamond knife. We floated the films from water onto copper grids and dried the sample in the vacuum at room temperature for 2 days. From Figure 2a and b, we clearly see that both the *l*-MWNTs and the *s*-MWNTs have a good dispersion within the PMMA matrix. The major difference between the two is that the *l*-MWNTs form an overlapping network in the polymer matrix, while the *s*-MWNTs are separated from each other without the formation of networks in the PMMA bulk.

Results and Discussion

We first investigated the qualitative influence of varying the length of MWNTs on the dewetting dynamics of polymer films. In parts a and b of Figure 3, we show optical microscope images of the dewetting holes produced in the PS films floated on the PMMA substrates and annealed at 195 °C for 2 and 4 h, respectively. After 2 h, fairly large holes have already formed in the control sample, which continue to grow with annealing time. For the 1% *l*-MWNT filled samples, we find that the dewetting holes do not appear until approximately 3 h of annealing at the same temperature (see Figure 3c), and then they open at a much slower rate and are still quite small even after 6 h of annealing. From Figure 3e and f, we can see that in the case of the 1% *s*-MWNT filled samples, we do not observe large holes after 3 h, but the surface of the film has roughened considerably. Closer examination with higher resolution indicates that many small holes have opened and the rough areas correspond to overlapping rims.

The microscopic structure of the holes was studied using atomic force microscopy. In the first row of Figure 4, we show topographical AFM images of samples annealed for 2 h. From the figure, we can clearly see that the control has the usual holes surrounded by rims. Much smaller holes with overlapping rims

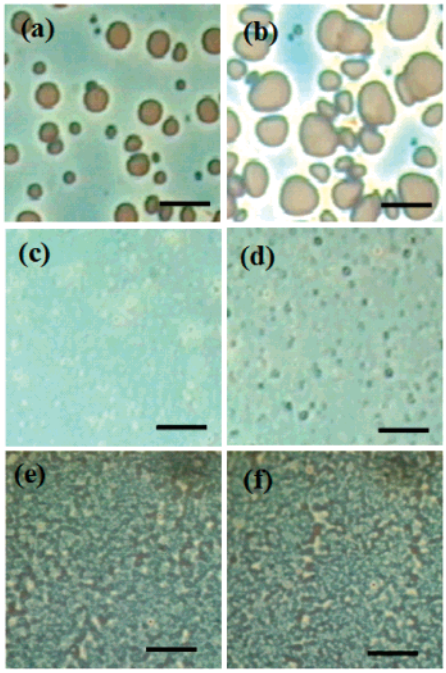

Figure 3. Typical optical microscope images of dewetting holes from a bilayer sample of a 4000K PS floated on a 62K PMMA layer after annealing at 195 °C for (a) 2 and (b) 4 h; PS on PMMA film with 1% *l*-MWNTs for (c) 3 and (d) 6 h; and 1% *s*-MWNTs for (e) 3 and (f) 6 h (scale bar = 20 μm).

are observed in the 1% *s*-MWNT sample, and nearly no holes at all are seen in the 1% *l*-MWNT sample, after the same annealing time for 2 h at 195 °C. After annealing for 24 h, adjacent holes in the control sample have coalesced forming droplet PS on the PMMA (see Figure 4d). In the case of the 1% *s*-MWNT, droplets have formed as well, although smaller in size. (From the figure, we see that the sample with *s*-MWNTs also has more holes on the surface, where each hole is nucleated on an agglomeration of short nanotubes (see Figure 4i).) Because the interactions between the tubes and the polymer are not attractive, the particles phase segregate and agglomerate upon dewetting as previously reported for films containing carbon black by Sharma et al.[7] The decreased rate of hole growth in this case can also be attributed to the higher density of holes, which overlap at a much earlier time. On the other hand, the long nanotubes are entangled and cannot move and form agglomerations within the matrix. The small amount of nucleating centers observed in these films corresponds to the impurities seen in the sample in Figure 2a. Even though we purified these nanotubes, a small amount remained, which segregated to the surface. In the case of the 1% *l*-MWNT samples annealed for 24 h (Figure 4e), the holes are now well defined. As compared to Figure 4g, which is annealed for 72 h, we see that they continue to grow very slowly. Hence, the nanotubes modify the effective viscosity of the lower layer, rather than affecting the degree of compatibilization. This can be further seen in the contact angle measurements. The Young's contact module is directly related to the interfacial width between the polymers. Here, we see that the final contact angles at equilibrium are nearly the same among all of the samples, and hence the presence of the tubes does not affect the chemical potential or the degree of miscibility between the polymers.

To calculate the viscosity of the bottom layer, the average diameters were measured from 8 to 10 holes and plotted as a function of the annealing time (t). According to the model developed by Brochard-Wyart et al.,[4] the dewetting velocity (V)

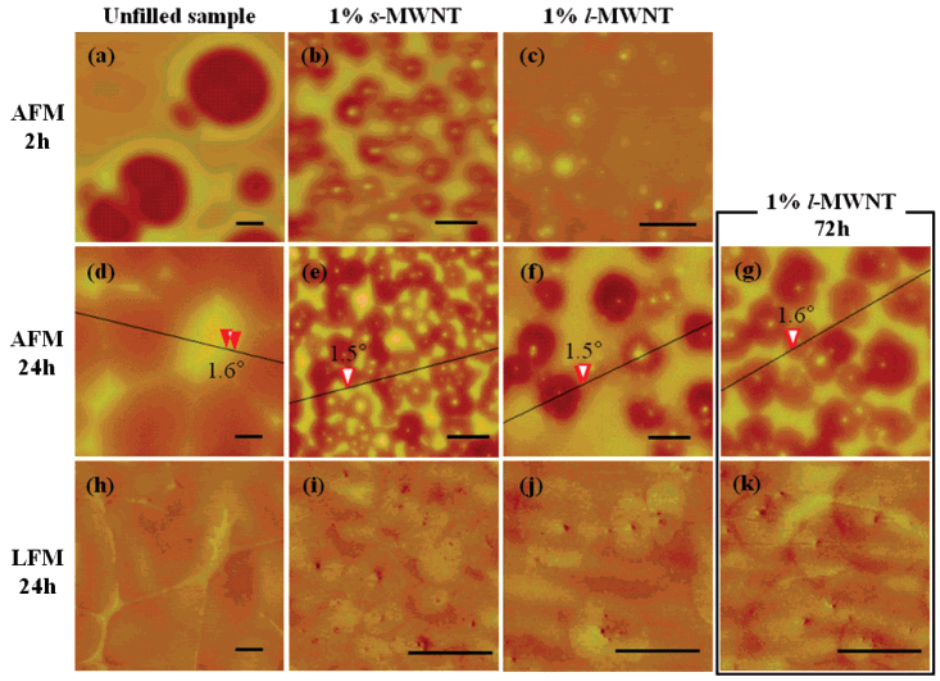

Figure 4. AFM images of dewetting holes of PS films on the PMMA substrates unfilled and filled with 1% *s*-MWNTs and *l*-MWNTs annealed at 195 °C for (a−c) 2, (d−f) 24, and (g) 72 h, and (h−k) their corresponding LFM image (scale bar = 2 μm).

in the liquid/liquid system depends on the relative viscosities of the PS and PMMA layers, respectively denoted as η_A and η_B, the surface and interfacial tension (γ_A, γ_B, and $\gamma_{A/B}$), and the thickness of the bottom and top layers, L and e, respectively. When two liquids slide along each other, the energy is dissipated in the less viscous layer. In this case, the viscosity of the upper PS layer is $\eta_A = 8.0 \times 10^8$ Ns/cm^2, and that of the lower (unfilled) PMMA layer is $\eta_B = 1.2 \times 10^5$ Ns/cm^2, or $\eta_A/\eta_B \approx 7 \times 10^3$ at 190 °C.[18,19] Hence $\eta_A >> \eta_B$, where the bottom layer behaves like a liquid and the dewetting hole growth is governed by η_B. Therefore, the PS and PMMA will be referred to the "probe" and "test" layers, respectively. For this case, Brochard-Wyart et al.[4] show that if L is smaller than the rim width (l), the hole diameter (R) is expected to grow with $t^{2/3}$ according to

$$R = \left(\frac{\gamma^2 L^2 \theta_e}{\eta_B{}^2 e}\right)^{1/3} t^{2/3} \quad (1)$$

and the velocities are then calculated to be

$$V = \left(\frac{\gamma^2 L^2 \theta_e}{\eta_B{}^2 e}\right)^{1/3} t^{-1/3} \quad (2)$$

where γ is the effective surface tension obtained from $1/\gamma = 1/\gamma_A + 1/\gamma_{A/B}$ and θ_e is the equilibrium contact angle. From the classical Neuman construction, θ_e can be obtained by $\theta_e = \theta_A + \theta_B$, where θ_A is the equilibrium apparent contact angle and θ_B is the Neuman angle below the liquid/liquid interface. θ_B is allowed to be calculated from the Neuman equation,[20]

$$\gamma_{A/B} \sin \theta_B = \gamma_A \sin \theta_A \quad (3)$$

In this study, we fixed the thickness of the bottom layer to be 1100 ± 50 Å, while the lateral size of the rim was approximately 2.5 μm. Henc, all samples met the requirements for the thin liquid substrate regime.

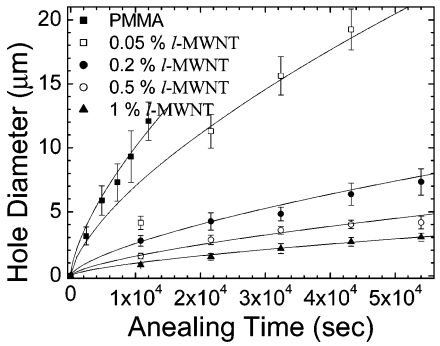

Figure 5. Dewetting hole diameter of PS/PMMA bilayers as a function of *l*-MWNT mass fraction and annealing time at 195 °C. The solid symbols are the actual data annealed at different times, and the solid lines are the best fits to eq 1.

The contact angle (θ_A) was measured from the slope of the profile close to the contact line. Figure 4d is the AFM topography image of the PS droplets on the PMMA layer at the late dewetting stage, where we find that θ_A is 1.6 ± 0.3°. 1% *s*-MWNT and 1% *l*-MWNT filled samples also have nearly the same contact angle of $\theta_A = 1.5 \pm 0.4°$ and 1.6 ± 0.4°, respectively. θ_B can be obtained by substituting the known values for $\gamma_{A/B}$, γ_A,[21] and the measured values for θ_A into eq 3, and θ_e ($=\theta_A + \theta_B$) was then substituted into eq 1 and fitted to the hole growth data. Figure 5a shows the dependence of the concentration of the *l*-MWNTs on dewetting hole growth as a function of the annealing time at 195 °C. As can be seen in the Figure 6a, good fits are obtained with the theoretical power law, and the holes grow as $t^{2/3}$ for all of the cases. From the figure, we also clearly see that the hole diameters grow more slowly as the concentration of the *l*-MWNTs increases under the same annealing condition. As we show later, the interactions between the nanotubes and the polymer matrix are negligible and the polymer chains move freely; therefore, we do not believe that the hindrance is due to any pinning effects.[8]

The effective viscosity (η_e) of the test layers can be calculated as a function of the nanotubes concentration from fits of eq 1. The results for both *l*-MWNTs and *s*-MWNTs are plotted in

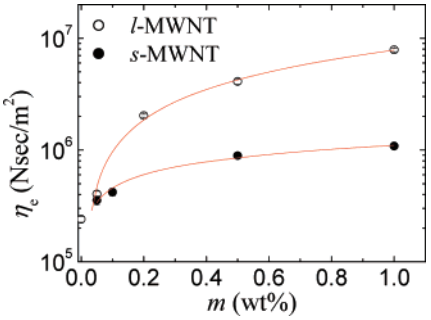

Figure 6. Thin film viscosity derived from dewetting measurement as a function of the concentration of nanotubes.

Figure 6a as a function of the weight fraction of both *l*-MWNTs and *s*-MWNTs, where we can see that at concentrations as low as 0.2%, η_e begins to increase sharply till it becomes approximately 30 and 4 times higher for the *l*-MWNT the s-MWNTs, respectively, as compared to the control sample at a concentration of 1%. This sudden change in the viscosity, followed by a plateau, can be interpreted as corresponding to a rheological percolation threshold above which the nanotubes physically hinder the motion of polymers, even in the absence of attractive surface interactions. Hough et al. and Du et al.[10,12] have used a power law relation between the viscosity and the mass fraction of the fillers:

$$\eta_e \propto (m - m^*)^{\nu} \tag{4}$$

where m is the MWNT mass fraction, m^* is the percolation threshold, and ν is the percolation exponent. The solid lines in Figure 6 are fits to eq 4 where we obtain nearly the same value of $m^* = 0.01\%$ for *l*-MWNT and *s*-MWNT samples; however, the percolation exponents, $\nu = 0.87$ and 0.36 for the *l*-MWNT and *s*-MWNT samples, are very different, indicating that *l*-MWNTs are much more effective than *s*-MWNTs at enhancing the viscoelastic response. Examining the TEM images, we therefore postulate that this difference would be ascribed to the formation of a nanotube network, as shown in Figure 2, which can only be formed by the *l*-MWNTs that can effectively entangle with each other. The *s*-MWNTs can still pose physical obstacles to the motion of the polymers, but because these nanotubes are not entangled, they are more mobile and hence not effective at preventing long-range motion.

To further investigate whether the mechanism is purely one of mechanical hindrance, we also investigate the effect of the MWNT on the tracer diffusion dynamics of isolated chains. Increased viscosity can also occur when attractive interactions exist, which can pin the polymer chains to the surface of the nanofiller. Hence, we chose to directly measure the effect of nanotube concentration for both short and long MWNTs on the tracer diffusion coefficient of the polymer chains, using neutron reflectivity. Figure 7 shows the neutron specular reflectivity profile for a bilayer sample (inset) consisting of PMMA (85K) film floated on top of a layer spun-cast on Si and consisting of 60 wt % of PMMA (85K) and 40 wt % of *d*PMMA (86.5K) film. Both layers, in each sample, were loaded with 0.2% of either long or short MWNTs annealed in situ at 138 °C for different times. A control sample without nanotubes was also annealed and measured under the same conditions. The thickness of both layers in each sample was greater than 5 times the radius of gyration (R_g) to ignore the effect of the polymer/substrate interaction on the interfacial dynamics at the center of the sample.[22,23] The data are shown in Figure 7, where the solid lines are fits to the profiles shown in the inset of Figure 8. Before

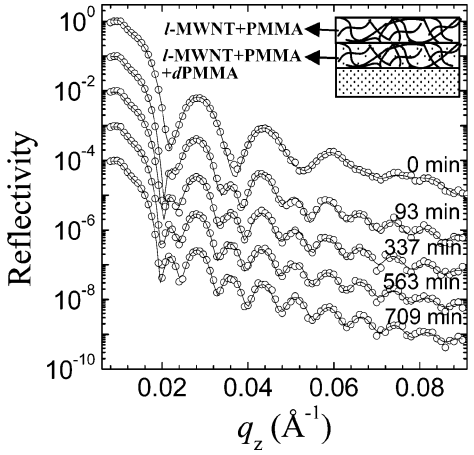

Figure 7. Typical neutron reflectivity data from the PMMA/*d*PMMA bilayer films with 0.2% of *l*-MWNTs in both top and bottom layers (schematic of the sample geometry was shown in the inset), annealed at 138 °C as a function of time. The solid lines are the best fits to data. Consecutive reflectivities have been offset from each other for clarity.

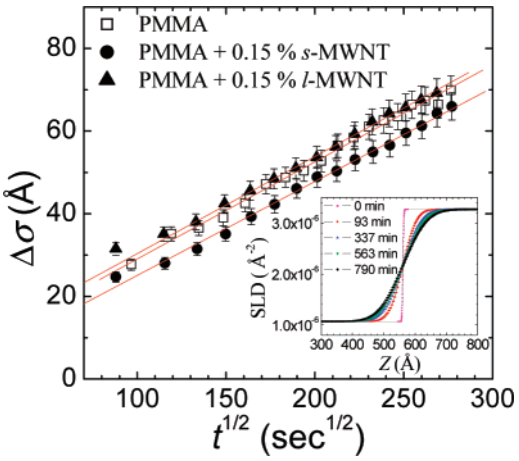

Figure 8. The rms roughness plotted as a function of the square root of the annealing time at 138 °C for the PMMA/*d*PMMA bilayer films unfilled and filled with 0.2% of *l*-MWNTs and *s*-MWNTs. The inset depicts corresponding scattering length density profiles as a function of the annealing time.

annealing, the reflectivity profile shows several distinct fringes with a periodicity corresponding to the thickness of the deuterated bottom layer. According to the fitted SLD profile, the initial interface is sharply defined as shown in the inset of Figure 8. As the sample is annealed, the interface of the bilayer begins to broaden till only a uniform frequency becomes visible, as the *d*PMMA has now diffused uniformly into both layers.

In the case of the Fickian diffusion,[24] the interface is expected to broaden with a scaling of one-half of time, $\Delta\sigma = 2(Dt)^{1/2}$, where D represents a diffusion coefficient, and $\Delta\sigma = (\sigma^2 - \sigma_0^2)^{1/2}$, where σ is interfacial rms roughness and σ_0 is initial rms roughness of the interface. In Figure 8, $\Delta\sigma$ was plotted as a function of the square root of annealing time at 138 °C for the PMMA/*d*PMMA bilayer samples unfilled and filled with 0.2% of *s*-MWNTs and *l*-MWNTs in both top and bottom layers. As can be seen in the figure, $\Delta\sigma$ scales linearly to the square root of time in all of the cases. From the slope of the fitted line, D is determined and tabulated in Table 2 where we find that D is unaffected by the addition of the nanotubes regardless of their length. Because both the long and the short nanotubes have the same surface functional groups, we can therefore conclude that the interactions between the nanotubes and the PMMA chains are not significant.

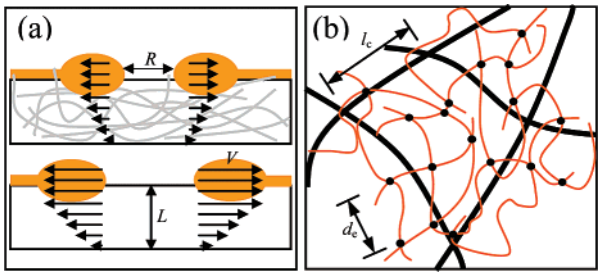

Figure 9. The effect of nanotube on the dewetting and diffusion dynamics. (a) The viscosity (η_e) of the bottom layer in the liquid−liquid dewetting regime is determined from dewetting velocity (V). Because the hole diameter (R) is larger than the network mesh size (ξ), the nanotubes act as the physical obstacles during the dewetting. Therefore, dewetting hole growth slows down, leading to the decrease in η_e. (b) Schematic view of the nanotube bundles and the entangled polymer melt where black circles correspond to chain entanglements. If the lattice constant of the nanotubes (l_c) is longer than the entanglement length (d_e), the motion follows the simple reptation model where diffusion dynamics is unaffected by the nanotube networks.

Table 2. Summary of the Diffusion Coefficients (D) of PMMA/*d*PMMA Bilayers with the MWNTs

	mass fraction (%)	annealing temperature (°C)	D ($\times 10^{-15}$ cm^2/s)
PMMA	0	138	2.21
s-MWNT	0.2	138	2.07
l-MWNT	0.2	138	2.21

The difference between the dewetting experiments and the diffusion experiments can then be understood in terms of the mesh size of nanotube networks. Hough et al.[12] have theoretically calculated the mesh size of nanotube networks with the simple equation $\xi = \sqrt{3/2\phi}d_c$, by assuming a cubic network, formed by infinitely long carbon nanotubes of diameter d_c, whose mesh size varies as the volume fraction according to $\phi = m/\epsilon$ where ϵ is the ratio of the densities of nanotube to polymer. In our case, because $d_c = 24$ nm and ϕ ranges from 2.8×10^{-4} to 5.5×10^{-3}, the corresponding range in ξ is from 380 to 1690 nm. This value can then be compared to the entanglement length (d_e) of the PMMA matrices, which is given by $d_e \leq bN_e$, where b is the statistical segment length ($b = 7.4$ Å) and N_e is the number of the monomer between entanglements of the PMMA chains ($N_e = 100$).[25,26] Hence, d_e ($\leq$74 nm) is always much less than ξ for all concentrations. If we take the nanotube network to be analogous to a cross-linked network swollen by free homopolymer, then de Gennes[27] has shown that if the length of the entanglements (d_e) is less than the distance between branch points (l_c) in the networks, the diffusion dynamics are independent of the gel network (satisfying the simple reptation model). Our samples are also in the regime where $d_e < l_c$, and the chain motion is mostly governed by the entanglements of chains rather than the nanotube networks (see Figure 9b). On the other hand, it is well known[27,28] that even a small amount of cross-links can greatly affect the overall chain mobility of the matrix where long-ranged motion occurs.

To probe this effect further, we also performed rheological measurements on bulk samples of PMMA containing both short and long MWNTs. Figure 10a shows the storage modulus at 200 °C as a function of the frequency (ω) for a 0.5% strain deformation of unfilled and filled samples with either 1% *s*-MWNTs or 1% *l*-MWNTs. From the figure, we can clearly see that even though both types of nanotubes enhance G' at low frequencies, the effect is larger for the *l*-MWNT filled samples. A similar enhancement of G' for long SWNTs was reported by Du et al.,[10] who attributed this behavior to nanotube network formation, as well.

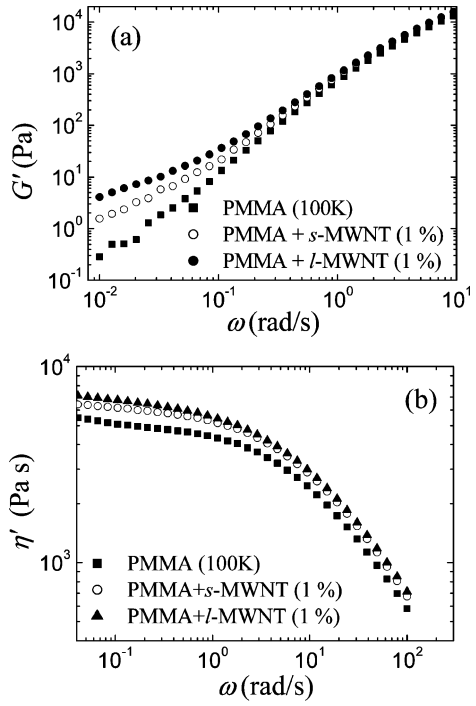

Figure 10. Master curves for the frequency dependence of (a) the storage modulus (G') and (b) the dynamic viscosity (η') for the PMMA bulks unfilled and filled with 1% of mass faction of *s*-MWNTs and *l*-MWNTs. Rheology performed at 200 °C and 0.5% strain.

To determine the viscosity, the loss modulus (G'') was measured and the dynamic viscosity ($\eta' = G''/\omega$) was plotted as a function of frequency in Figure 10b. The zero shear viscosity (η_0) was then extrapolated from the data from η' in the terminal region,[29] where

$$\eta_0 = \lim_{\omega \to 0} \eta' = \lim_{\omega \to 0} G''/\omega$$

and we find that, despite the larger differences in G', the differences in η_0 were minimal between the filled samples and the control.

The relative values of η_0 can be also directly compared to the diffusion results through the Einstein relationship:[30]

$$D = \frac{k_B T}{\eta_0 k_B / G(M) F(M,v)} \quad (5)$$

where $G(M)$ depends on the entanglement molecular weight and $F(M,v)$ is a function of the microstructural parameters of the polymer. From the diffusion and bulk rheological results, we find that both D and η_0 are consistently unaffected by the presence of the MWNTs regardless of their length because the interactions between the nanotubes and the PMMA matrix are at best very weak.

Finally, we also investigated the underlying morphology of the dewetted PMMA films after removing the top PS layer with cyclohexane. Li et al.[31] have recently shown that when the shear rate, $\dot{\gamma}$ ($=V/L$), of the dewetting layer is faster than the reptation time (τ) of the test layer, melt fracture can occur similar to the Sharkskin phenomenon observed for rapid extrusion in the bulk. In the unfilled sample, we clearly see that the opening holes have produced a depression in the substrate (see Figure 11a), similar to the melt fracture observed previously by Li et al.[31] and Qu et al.[32] The degree of melt fracture is much smaller in the sample with the 1% *s*-MWNTs (see Figure 11b) and completely eliminated in the sample with the 1% *l*-MWNTs

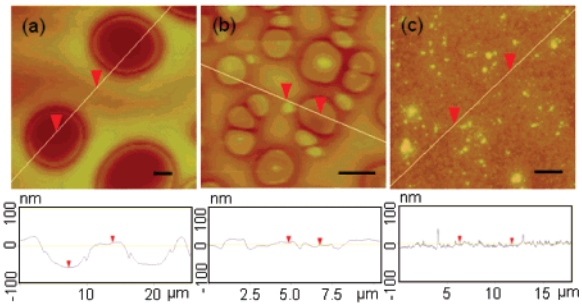

Figure 11. The samples were annealed for 2 h at 195 °C, and then immersed in cyclohexane to wash the top PS layer. AFM images are the underlying structure of the PMMA substrates (a) unfilled and filled with (b) 1% *s*-MWNTs and (c) 1% *l*-MWNTs. The cross-sectional traces correspond to the lines drawn across the figures. The height differences are 62 nm for the control, 8 nm for the *s*-MWNT, and ~0.5 nm for the *l*-MWNT, or no fracture was detected, within the experimental error due to capillary roughness of approximately 1 nm.

(see Figure 11c). The reptation time (τ) of the polymer chains in a melt is related to the tracer diffusion coefficient by $\tau_{rep} = l^2/2D$, where $l \approx aN/N_e$ is the length of the confining tube (reptation) and $a \approx bN_e^{1/2}$ is the tube diameter.[33] Because no pinning interactions are present, D is unchanged, and hence τ_{rep} (=443 s) is also unaffected. The shear rate of the PMMA dewetting layer in the absence of filler is $\dot{\gamma} = 4.2 \times 10^{-3} \pm 0.3 \times 10^{-3}$ s^{-1} and the associated time constant, $\tau = 1/\dot{\gamma} = 238 \pm 70$ s where $\tau < \tau_{rep}$. Hence, as is discussed in ref 31, the substrate film behaves in a rigid manner and a melt fracture occurs. In the case of the short nanotubes, $\tau_{short} = 1/\dot{\gamma} = 555 \pm 80$ s where $\tau_{short} \approx \tau_{rep}$, and the melt fracture still is observed, but the magnitude is greatly decreased. In the case of the nanotubes network, the shear rate is much slower, and the time constant is longer, $\tau_{network} = 1/\dot{\gamma} = 2631 \pm 350$ s or $\tau_{network} \approx 6\tau_{rep}$. The polymer has enough time to flow following the shear, and melt fracture does not occur.

Conclusions

We have investigated the effect of short and long MWNT on the viscosity of polymer films. When long-ranged motion occurs, as is the case in dewetting, the long nanotubes were more effective in increasing the viscosity than were the short nanotubes. The tracer diffusion coefficient was unaffected by the presence of the nanotubes network, indicating that interactions between the tubes and the polymer were weak. Furthermore, because the mesh of the network was much larger than the entanglement length, the diffusion of individual polymer chains was not affected. The data were interpreted in terms of a model whereby the long nanotubes formed an entangled network, which produced a physical barrier to the flow of the polymer, over length scales larger than the mesh size. Short nanotubes were unable to form these networks, and hence, even though they still provided some physical barriers to the flow, they were much less effective at preventing dewetting dynamics. Because the networks did not alter the interfacial energy between the polymers, they did not affect the equilibrium phase separated state, or the final contact angle. They only provided a barrier to plug flow thereby decreasing the dewetting velocity. We show that this had a distinct advantage in decreasing the interfacial shear rate and hence preventing melt fracture in the underlying film.

Acknowledgment. The authors thank Dr. Dilip Gersappe for helpful discussions. This work was supported by a grant from the NSF-MRSEC, Korea Research Foundation (D00058), and "the Center for Nanostructured Materials Technology" under the "21st Century Frontier R&D Program", BAERI, and Advanced Radiation Technology Inst., Jeongeup.

References and Notes

(1) Wang, W.-C.; Vora, R. H.; Kang, E.-T.; Neoh, K.-G.; Ong, C.-K.; Chen, L.-F. *Adv. Mater.* **2004**, *16*, 54.
(2) Dittinhhsud, H.; Tessler, N.; Friend, R. H. *Science* **1998**, *280*, 1741.
(3) Siegel, R. W. *Mater. Sci. Eng., A* **1993**, *168*, 189.
(4) Brochard-Wyart, F.; Martin, P.; Redon, C. *Langmuir* **1993**, *9*, 3682.
(5) Barnes, K. A.; Karim, A.; Douglas, J. F.; Nakatani, A. I.; Gruell, H.; Amis, E. J. *Macromolecules* **2000**, *33*, 4177.
(6) Xavier, J. H.; Sharma, S.; Seo, Y. S.; Isseroff, R.; Koga, T.; White, H.; Ulman, A.; Shin, K.; Satija, S. K.; Sokolov, J.; Rafailovich, M. H. *Macromolecules* **2006**, *39*, 2972.
(7) Sharma, S.; Rafailovich, M. H.; Peiffer, D.; Sokolov, J. *Nano Lett.* **2001**, *1*, 511.
(8) Luo, H.; Gersappe, D. *Macromolecules* **2004**, *37*, 5792.
(9) Pötschke, P.; Fornes, T. D.; Paul, D. R. *Polymer* **2002**, *43*, 3247.
(10) Du, F.; Scogna, R. C.; Zhou, W.; Brand, S.; Fisher, J. E.; Winey, K. I. *Macromolecules* **2004**, *37*, 9048.
(11) Kashiwagi, T.; Du, F.; Douglas, J. F.; Winey, K. I.; Harris, R. H.; Shields, J. R. *Nat. Mater.* **2005**, *4*, 928.
(12) Hough, L. A.; Islam, M. F.; Janmey, P. A.; Yodh, A. G. *Phys. Rev. Lett.* **2004**, *37*, 9048.
(13) Liu, J.; Rinzler, A. G.; Dai, H.; Hafner, J. H.; Bradley, R. K.; Boul, P. J.; Lu, A.; Iverson, T.; Shelimov, K.; Huffman, C. B.; Rodriguez-Macias, F.; Shon, Y.; Lee, T. R.; Colbert, D. T.; Smalley, R. E. *Science* **1998**, *280*, 1253.
(14) Lin, Y.; Rao, A. M.; Sadanadan, B.; Kenik, E. A.; Sun, Y.-P. *J. Phys. Chem. B* **2002**, *106*, 1294.
(15) Chen, X.; Yoon, K.; Burger, C.; Sics, I.; Fang, D.; Hsiao, B. S.; Chu, B. *Macromolecules* **2005**, *38*, 3883.
(16) Ton-That, C.; Shard, A. G.; Daley, S. R.; Brandley, R. H. *Macromolecules* **2000**, *33*, 8453.
(17) Du, F.; Fisher, J. E.; Winey, K. I. *J. Polym. Sci., Part B: Polym. Phys.* **2003**, *41*, 3333.
(18) Fuchs, K.; Friedrich, C.; Weese, J. *Macromolecules* **1996**, *26*, 5893.
(19) Li, C.; Koga, T.; Li, C.; Jiang, J.; Sharma, S.; Narayanan, S.; Lurio, L. B.; Hu, X.; Jiao, X.; Shinha, S. K.; Billet, S.; Sosnowik, D.; Kim, H.; Sokolov, J. C.; Rafailovich, M. H. *Macromolecules* **2005**, *38*, 5144.
(20) Slep, D.; Asselta, J.; Rafailovich, M.; Sokolov, J.; Winesett, A.; Smith, A. P.; Ade, H.; Anders, S. *Langmuir* **2000**, *16*, 2369.
(21) Brandrup, J.; Immergut, E. H.; et al. *Polymer Hand Book*, 2nd ed.; Wiley-Interscience: New York, 1989.
(22) Lin, E. K.; Kolb, R.; Satija, S. K.; Wu, W. *Macromolecules* **1999**, *32*, 3753.
(23) Li, C.; Kim, H.; Jiang, J.; Li, C.; Koga, T.; Lurio, L.; Schwarz, S.; Narayanan, S.; Lee, H.; Lee, Y. J.; Jiang, Z.; Sinha, S.; Rafailovich, M. H.; Sokolov, J. C. *Europhys. Lett.* **2006**, *73*, 899.
(24) Doi, M.; Edwards, S. F. *The Theory of Polymer Dynamics*; Clarendon Press: Oxford, UK, 1986.
(25) Rottler, J.; Robbins, M. O. *Phys. Rev. E* **2003**, *68*, 011801.
(26) Mark, J. E. *Physical Properties of Polymers Handbook*; American Institute of Physics: New York, 1996.
(27) de Gennes, P.-G. *Macromolecules* **1986**, *19*, 1245.
(28) de Gennes, P.-G. *Scaling Concepts in Polymer Physics*; Cornell University Press: New York, 1979.
(29) Rubinstein, M.; Colby, R. H. *Polymer Physics*; Oxford University Press: New York, 2003.
(30) Green, P. F.; Kramer, E. J. *J. Mater. Res.* **1986**, *1*, 202.
(31) Li, C.; Jiang, J.; Rafailovich, M. H.; Sokolov, J. C. *Europhys. Lett.* **2006**, *76*, 870.
(32) Qu, S.; Clarke, C. J.; Liu, Y.; Rafailovich, M. H.; Sokolov, J.; Phelan, K. C.; Krausch, G. *Macromolecules* **1997**, *30*, 3640.
(33) Zheng, X.; Sauer, B. B.; Van Alsten, J. G.; Schwarz, S. A.; Rafailovich, M. H.; Sokolov, J.; Rubinstein, M. *Phys. Rev. Lett.* **1995**, *74*, 407.

MA071550L